VI International Conference on Adaptive Modeling and Simulation
ADMOS 2013
J. P. Moitinho de Almeida, P. Díez, C. Tiago and N. Parés (Eds)

ON THE KINEMATIC STABILITY OF HYBRID EQUILIBRIUM TETRAHEDRAL MODELS

EDWARD A. W. MAUNDER*, JOSÉ P. MOITINHO DE ALMEIDA† AND ORLANDO J.B.A. PEREIRA†

* College of Engineering, Mathematics and Physical Sciences, University of Exeter
Harrison Building, North Park Road, Exeter EX4 4QF, UK
e-mail: e.a.w.maunder@exeter.ac.uk

† Department of Civil Engineering, Architecture and Georesources
Instituto Superior Técnico, Technical University of Lisbon,
Av. Rovisco Pais, 1049-001 Lisboa, Portugal
email: moitinho@civil.ist.utl.pt; orlando@civil.ist.utl.pt

Key words: Equilibrium models, tetrahedral elements, kinematic stability.

Summary. *This paper is concerned with establishing the nature of the kinematic instabilities that arise in tetrahedral hybrid equilibrium models when the elements are formulated with polynomial approximation functions of a general degree. The instabilities are due to the spurious kinematic (or zero energy) modes, and these modes are first derived for a single element. The paper continues by identifying those spurious modes that can be propagated from one element to another via an interface. It is shown that at least three such modes exist for all degrees.*

1 INTRODUCTION

Hybrid equilibrium elements have been used to generate dual analyses for error estimation of conforming models[1]. Dual analyses may involve reanalysis of a complete mesh, or may involve local analyses of star patches[2]. In any event it becomes important to know whether spurious kinematic modes associated with hybrid equilibrium models may exist, and if so, whether they will affect the dual analyses. These questions have been studied for plate elements[3-5]. In this paper, we investigate the form taken by spurious kinematic modes for a single tetrahedral element of general polynomial degree, and consider the propagation of these modes between a pair of adjacent elements of the same degree. The results of this investigation should help to determine the general kinematic stability of patches of tetrahedral elements[6,7], thereby setting the basis for robust implementations of these approaches. The definition of spurious modes associated with an edge and an interface of an element exploit an orthogonal basis of polynomials for a triangular face[8] that are expressed in terms of area coordinates. These enable the spurious modes to be generated in a hierarchical fashion which takes advantage of cyclic symmetry.

2 GENERAL FEATURES OF SPURIOUS KINEMATIC MODES OF TETRAHEDRA

Spurious kinematic modes refer to boundary displacements that have the nature of pseudo-mechanisms and cause no internal stress. They do zero work with admissible boundary tractions, which are those that equilibrate with internal stress fields. Displacements of a face of a tetrahedron are described by complete polynomials of degree *d*, and this implies that the dimensions of the spaces of displacements and rigid body modes for an element are defined in Equation (1). Internal stress fields are described by polynomials of the same degree, and complete within the constraints set by equilibrating with zero body forces. In this case the dimensions of the stress and hyperstatic stress spaces are given by[9] Equation (2).

$$n_v = 4\times 3\times 0.5(d+1)(d+2);\; n_{rbm} = 6 \tag{1}$$

$$n_s = 0.5(d+1)(d+2)(d+6);\; n_{hyp} = 0.2(d-3)(d-2)(d+2) \text{ for } d>2 \tag{2}$$

and then the number of independent spurious kinematic modes is given by Equation (3).

$$n_{skm} = (n_v - n_{rbm}) - (n_s - n_{hyp}) = 6(d+1) \text{ for } d>2\,. \tag{3}$$

When $d \leq 2$, the element is isostatic and then:

$$n_{skm} = 0.5(d+1)(d+2)(6-d) - n_{rbm}\,. \tag{4}$$

Tractions applied to the boundary are considered as belonging to a space dual to that of displacements. Admisible tractions are those that equilibrate with an internal stress field, and the necessary and sufficient conditions for admissibility correspond to the need for complementary shear stresses along an edge of a tetrahedral element. With reference to Figure 1, the complementary shear stress condition along edge 3-4 has the form in Equation (5).

$$\sin\varphi\cdot\tau_{1n} - \cos\varphi\cdot\sigma_1 + \sin\varphi\cdot\tau_{2n} + \cos\varphi\cdot\sigma_2 = 0\,, \tag{5}$$

where φ is the dihedral angle between faces adjacent to the edge. For traction fields of degree $d \geq 2$, $(d+1)$ independent conditions associated with each edge lead to the homogeneous admissibility conditions on generalised element tractions represented by vector $\boldsymbol{g}$, i.e. $\boldsymbol{A}^T\boldsymbol{g} = \boldsymbol{0}$ where the dimensions of $\boldsymbol{A}$ are $n_v \times n_{skm}$. The spurious kinematic modes are then defined in terms of the dual basis for displacements by the columns of $\boldsymbol{A}$.

3 SPURIOUS KINEMATIC MODES FOR A TETRAHEDRAL ELEMENT OF GENERAL DEGREE

A convenient basis for polynomial displacement or traction functions over a triangular face is derived from the functions in the *Digital Library of Mathematical Functions* [8]. These $n = 0.5(d+1)(d+2)$ functions have the properties of orthogonality and the benefit of a hierarchical structure. When expressed in terms of area coordinates L_i they can be organised in a vector $\boldsymbol{h}$ to give Legendre polynomials along a particular edge, which leads to a very simple form of $\boldsymbol{A}$ when it is restricted to the two faces adjacent to that edge. This form, with dimensions $(4n\times(d+1))$, is defined by $\bar{A}$ in Equation (6), e.g. for the edge where $L_1 = 0$.

$$\bar{\boldsymbol{A}} = \left[\begin{array}{c} \sin\varphi \cdot \Delta_1^{-1}\boldsymbol{HJ} \\ -\cos\varphi \cdot \Delta_1^{-1}\boldsymbol{HJ} \\ \hline \sin\varphi \cdot \Delta_2^{-1}\boldsymbol{H} \\ \cos\varphi \cdot \Delta_2^{-1}\boldsymbol{H} \end{array}\right] \tag{6}$$

where Δ_1 and Δ_2 are the areas of faces 1 and 2 in Figure 1, $\boldsymbol{J} = \boldsymbol{I}_{(d+1)}$ with even numbered diagonal coefficients = -1, and the $n\times(d+1)$ matrix $\boldsymbol{H}$ and the n dimensional vector $\boldsymbol{h}$ are defined in Equation (7).

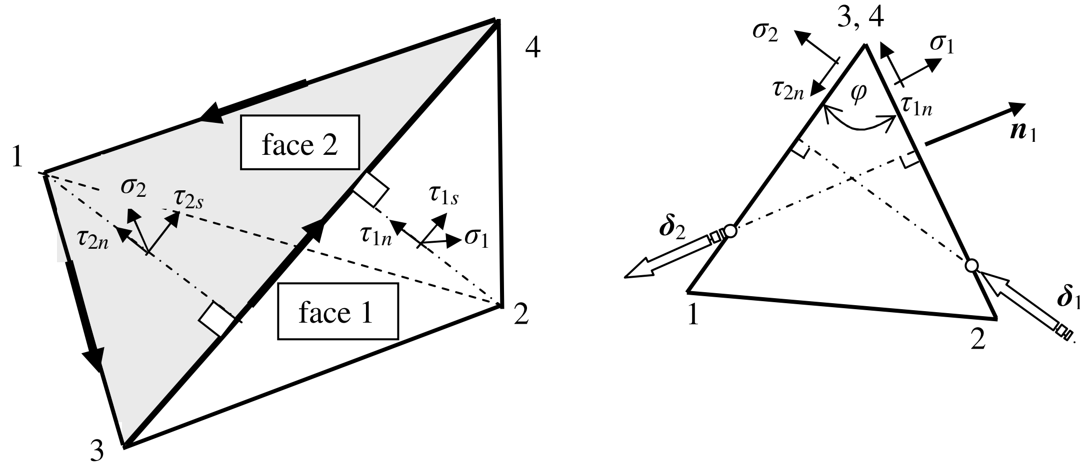

Figure 1: Traction components on a tetrahedron relative to edge connecting vertices 3 and 4. The right hand view is projected from vertex 3 to vertex 4.

$$\boldsymbol{H} = \left[\begin{array}{ccccc} 2 & 0 & 0 & \cdots & 0 \\ \hline 4 & 0 & 0 & \cdots & 0 \\ 0 & 12 & 0 & \cdots & 0 \\ \hline 6 & 0 & 0 & \cdots & 0 \\ 0 & 18 & 0 & \cdots & 0 \\ 0 & 0 & 30 & 0 & \cdots \\ \hline 8 & 0 & 0 & 0 & \cdots \\ 0 & 24 & 0 & 0 & \cdots \\ 0 & 0 & 40 & 0 & \cdots \\ 0 & 0 & 0 & 56 & \cdots \\ \hline \ddots & \ddots & \ddots & \ddots & \ddots \end{array}\right] \text{ when } \boldsymbol{h} = \left\{\begin{array}{c} 1 \\ \hline 1-3L_1 \\ -L_2+L_3 \\ \hline 1+2L_1(-4+5L_1) \\ (-1+5L_1)(L_2-L_3) \\ L_2^2-4L_2L_3+L_3^2 \\ \hline 1-5L_1(3+L_1(-9+7L_1)) \\ (1+3L_1(-4+7L_1))(-L_2+L_3) \\ (1-7L_1)\left(L_2^2-4L_2L_3+L_3^2\right) \\ -(L_2-L_3)\left(L_2^2-8L_2L_3+L_3^2\right) \\ \hline \vdots \end{array}\right\} \tag{7}$$

Similar bases of $\boldsymbol{h}$ for other edges of the face are obtained using cyclic symmetry. Then the m^{th} column of $\boldsymbol{H}$ defines a signature function k_{2e}^{m} for face 2 corresponding to edge e as a combination of the basis functions in $\boldsymbol{h}$. The total displacement vector of a point in face 2 due to the spurious kinematic modes associated with its three edges, oriented as in Figure 1, is given by Equation (8), where $\boldsymbol{n}_e$ is the unit outward normal vector to the other face adjacent to edge e, and a_e^m is the amplitude of the mth spurious mode associated with edge e.

$$\boldsymbol{\delta}_2 = \left(-\frac{1}{\Delta_2} \sum_m \sum_e k_{2e}^m \cdot a_e^m \right) . \boldsymbol{n}_e \tag{8}$$

4 PROPAGATION OF "MALIGNANT" SPURIOUS MODES BETWEEN TETRAHEDRAL ELEMENTS.

Propagation of spurious kinematic modes can occur between a pair of elements A and B when they result in compatible displacements at the interface. The displacements are resolved into in-plane and normal components as indicated in Figure 2 at a point P. For each signature function k_{je}^m displacements are evaluated at a set of n grid points with a common set of rigid body constraints. This leads to the displacement Equation (9) for element A.

$$\boldsymbol{u} = \boldsymbol{E^A} \cdot \boldsymbol{a^A} \quad \text{and} \quad w = \boldsymbol{C^A} \cdot \boldsymbol{a^A} \tag{9}$$

where $\boldsymbol{E^A}$ and $\boldsymbol{C^A}$ contain displacement components corresponding to spurious modes of unit amplitude, and have dimensions ($2n$×$3(d+1)$) and (n×$3(d+1)$) respectively. The amplitudes of the spurious modes are collected in the vector $\boldsymbol{a^A}$. The matrices can be expressed as in Equation (10), where the diagonal matrices are defined in terms of the Kronecker products in Equation (11) and φ_e^A denotes the dihedral angle at edge e of element A.

$$\boldsymbol{E^A} = \left[\boldsymbol{E}_1 \mid \boldsymbol{E}_2 \mid \boldsymbol{E}_3\right]\boldsymbol{D_s^A} = \boldsymbol{E} \cdot \boldsymbol{D_s^A}, \text{ and } \boldsymbol{C^A} = \left[\boldsymbol{C}_1 \mid \boldsymbol{C}_2 \mid \boldsymbol{C}_3\right]\boldsymbol{D_c^A} = \boldsymbol{C} \cdot \boldsymbol{D_c^A} \tag{10}$$

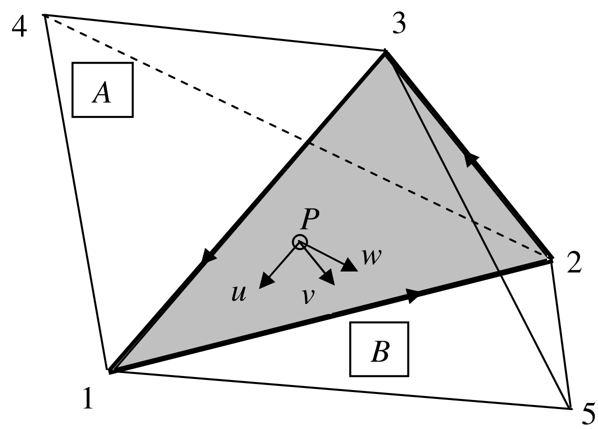

Figure 2: Interface between elements A and B.

Matrices $\boldsymbol{E}$ and $\boldsymbol{C}$ are partitioned in Equation (10) to match the coefficients from edges 1 to 3. Since these matrices are only dependent on the signature functions, which are expressed in terms of area coordinates, they are independent of the shape of the interface or the dihedral angles.

$$\boldsymbol{D}_s^{\boldsymbol{A}} = \frac{1}{2\Delta}\begin{bmatrix} \sin\varphi_1^{\boldsymbol{A}} & 0 & 0 \\ 0 & \sin\varphi_2^{\boldsymbol{A}} & 0 \\ 0 & 0 & \sin\varphi_3^{\boldsymbol{A}} \end{bmatrix} \otimes \boldsymbol{I}_{d+1} \text{ and } \boldsymbol{D}_c^{\boldsymbol{A}} = \frac{1}{2\Delta}\begin{bmatrix} \cos\varphi_1^{\boldsymbol{A}} & 0 & 0 \\ 0 & \cos\varphi_2^{\boldsymbol{A}} & 0 \\ 0 & 0 & \cos\varphi_3^{\boldsymbol{A}} \end{bmatrix} \otimes \boldsymbol{I}_{d+1}. \tag{11}$$

Compatibility conditions take the form in Equation (12), where the vector $\lfloor \boldsymbol{a}^{\boldsymbol{A}} \mid \boldsymbol{a}^{\boldsymbol{B}} \rfloor^{\boldsymbol{T}}$ contains the amplitudes of the 6(d+1) spurious modes associated with the edges of the interface belonging to elements A and B. The diagonal matrices $\boldsymbol{D}_s^{\boldsymbol{B}}$ and $\boldsymbol{D}_c^{\boldsymbol{B}}$ for element B are similar to those for element A, but involve the dihedral angles φ_e^B.

$$\left[\begin{array}{c|c} \boldsymbol{E}\boldsymbol{D}_s^{\boldsymbol{A}} & -\boldsymbol{E}\boldsymbol{D}_s^{\boldsymbol{B}} \\ \hline \boldsymbol{C}\boldsymbol{D}_c^{\boldsymbol{A}} & \boldsymbol{C}\boldsymbol{D}_c^{\boldsymbol{B}} \end{array}\right]\left\{\begin{array}{c} \boldsymbol{a}^{\boldsymbol{A}} \\ \hline \boldsymbol{a}^{\boldsymbol{B}} \end{array}\right\} = \left\{\begin{array}{c} \boldsymbol{0} \\ \hline \boldsymbol{0} \end{array}\right\} \tag{12}$$

It is found that generally ($d \geq 2$) $\boldsymbol{E}$ has full column rank and so any spurious mode involves in-plane deformation of the interface, and compatibility requires $\boldsymbol{D}_s^{\boldsymbol{A}} \cdot \boldsymbol{a}^{\boldsymbol{A}} = \boldsymbol{D}_s^{\boldsymbol{B}} \cdot \boldsymbol{a}^{\boldsymbol{B}}$. Eliminating $\boldsymbol{a}^{\boldsymbol{A}}$ from the second set of Equation (12), leads to Equation (13).

$$\boldsymbol{C}\left[\boldsymbol{D}_{\cot}^{\boldsymbol{A}} + \boldsymbol{D}_{\cot}^{\boldsymbol{B}}\right]\left[\boldsymbol{D}_s^{\boldsymbol{B}}\right]\boldsymbol{a}^{\boldsymbol{B}} = \boldsymbol{0} \tag{13}$$

where the suffix "cot" implies that $\cot\varphi_e$ replaces $\cos\varphi_e$ or $\sin\varphi_e$ in the diagonal matrices. The consequence of Equation (13) is that compatibility can be satisfied:

- when $\boldsymbol{C}$ is column rank deficient, and/or
- the geometrical configuration is degenerate in the sense that $\cot\varphi_e^A + \cot\varphi_e^B = 0$ for one or more dihedral angles, i.e. faces in adjacent elements are coplanar.

Numerical trials involving singular value decomposition reveal that, when $d > 3$, $\boldsymbol{C}$ has column rank 3d and hence 3 spurious kinematic modes can be propagated via the interface in the non-degenerate case. These modes are linearly related to independent solutions of the homogeneous equations $\boldsymbol{Ca} = \boldsymbol{0}$, and such solutions are given by the 3×3(d+1) matrix in Equation (14).

$$\boldsymbol{a}^{\boldsymbol{T}} = \left[\begin{array}{ccccc|ccccc|ccccc} 0 & 1 & 0 & 1 & \cdots & -1 & 0 & -1 & 0 & \cdots & 1 & 0 & 1 & 0 & \cdots \\ 1 & 0 & 1 & 0 & \cdots & 0 & 1 & 0 & 1 & \cdots & -1 & 0 & -1 & 0 & \cdots \\ -1 & 0 & -1 & 0 & \cdots & 1 & 0 & 1 & 0 & \cdots & 0 & 1 & 0 & 1 & \cdots \end{array}\right]. \tag{14}$$

The corresponding spurious mode amplitudes for element A can then be defined in Equation (15).

$$\boldsymbol{a}^{\boldsymbol{A}} = \frac{1}{\Delta^2}\left[\boldsymbol{D}_s^{\boldsymbol{A}}\right]^{-1}\left[\boldsymbol{D}_{\cot}^{\boldsymbol{A}} + \boldsymbol{D}_{\cot}^{\boldsymbol{B}}\right]^{-1}\boldsymbol{a}\,. \tag{15}$$

This solution can also be expressed, using the Kronecker matrix product in Equation (16).

$$\boldsymbol{a}^{\boldsymbol{A}} = \begin{bmatrix} \dfrac{\sin\varphi_1^{\boldsymbol{B}}}{\sin\left(\varphi_1^{\boldsymbol{A}}+\varphi_1^{\boldsymbol{B}}\right)} & 0 & 0 \\ 0 & \dfrac{\sin\varphi_2^{\boldsymbol{B}}}{\sin\left(\varphi_2^{\boldsymbol{A}}+\varphi_2^{\boldsymbol{B}}\right)} & 0 \\ 0 & 0 & \dfrac{\sin\varphi_3^{\boldsymbol{B}}}{\sin\left(\varphi_3^{\boldsymbol{A}}+\varphi_3^{\boldsymbol{B}}\right)} \end{bmatrix} \otimes \boldsymbol{I}_{d+1}\cdot\boldsymbol{a} \tag{16}$$

It is observed from the form of $\boldsymbol{a}^T$ that the three modes can be characterised by a single one, which generates two more independent ones by using cyclic symmetry. When the pair of elements are symmetrical about the interface, $\boldsymbol{D}_{\mathrm{cot}}^{\boldsymbol{A}} = \boldsymbol{D}_{\mathrm{cot}}^{\boldsymbol{B}}$ and in this case $\boldsymbol{C}\boldsymbol{D}_{\boldsymbol{c}}^{\boldsymbol{A}}\cdot\boldsymbol{a}^{\boldsymbol{A}} = \boldsymbol{0}$ and consequently the interface remains plane. The characteristic mode for a pair of regular tetrahedra of degree 4 is illustrated by the in-plane displacements shown in Figure 3.

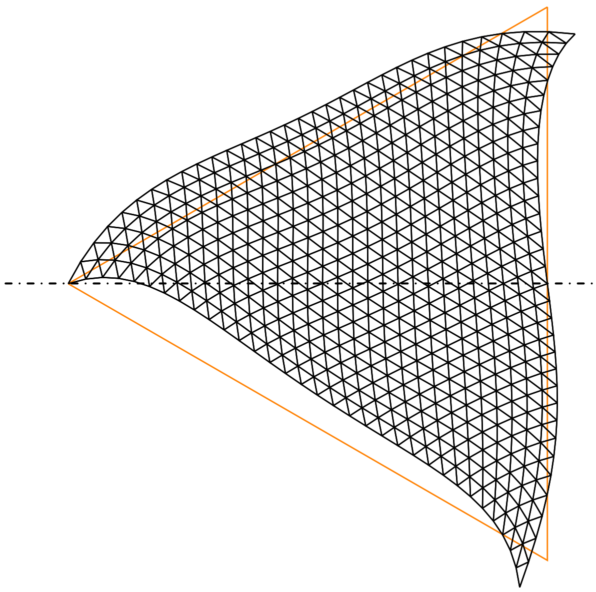

Figure 3: Characteristic spurious kinematic mode that can be propagated between a pair of regular tetrahedral elements of degree 4.

The number of malignant modes for non-degenerate cases increases for $d < 4$, and the complete set of numbers is presented in Table 1.

Table 1: Number of malignant modes for a general degree.

d	0	1	2	3	≥ 4
number of malignant modes	3	6	6	5	3

It should be noted that when:

d = 1, rank($\boldsymbol{E}$) = 3, and the 6 spurious modes associated with the interface of one of the elements can freely exist in a state of constant strain coupled with a rigid body displacement. Thus only 3 of the combined modes can be propagated to involve deformations.

d = 0, the 3 spurious modes associated with the interface of one of the elements can freely exist as rigid body translations. Thus all the modes can be freely propagated as rigid body modes.

5. CLOSURE

A pair of tetrahedral hybrid equilibrium elements always has the potential for at least three spurious kinematic modes to be propagated from one element to the other. This feature of 3D tetrahedral models is more complicated than the case with 2D models with triangular elements, where such propagation is normally blocked for degrees greater than two.
Thus establishing the existence of spurious kinematic modes in a pair of tetrahedral elements is just the first stage in understanding when and how these modes can propagate in a more general mesh. Whilst experience has shown[6] that assemblies of four tetrahedra into a single macro-element is free of spurious kinematic modes, it is intended to pursue further research to address the stability of more general configurations.

REFERENCES

[1] Almeida JPM, Pereira OJBA. Upper bounds of the error in local quantities using equilibrated and compatible finite element solutions for linear elastic problems. *Comp. Meth. Appl. Mech. Engng.* (2006),**195**:279-296.
[2] Almeida JPM, Maunder EAW. Recovery of equilibrium on star patches using a partition of unity technique. *Int. J. Num. Meth. Engng.* (2009) **79**:1493-1516.
[3] Maunder EAW, Almeida JPM. A triangular hybrid equilibrium plate element of general degree. . *Int. J. Num. Meth. Engng.* (2005) **63**:315-350.
[4] Maunder EAW, Almeida JPM. The stability of stars of triangular equilibrium plate elements. . *Int. J. Num. Meth. Engng.* (2009) **77**:922-968.
[5]Maunder EAW. On the stability of hybrid equilibrium and Trefftz finite element models for plate bending problems. *Comp. Ass. Mech. Engng. Sci.* (2008) **15**, 279-288.
[6] Almeida JPM, Pereira OJBA, A set of hybrid equilibrium finite element models for the analysis of three-dimensional solids. *Int. J. Num. Meth. Engng*. (1996) **39,** 2789-2802.
[7] Pereira OJBA, Hybrid equilibrium hexahedral elements and super-elements. *Commun. Numer. Meth. Engng*. (2008) **24**, 157-165.
[8] National Institute of Standards and Technology *Digital Library of Mathematical Functions*, http://dlmf.nist.gov/18.37.E7, Release 1.0.5 of 2012-10-01.
[9] Kempeneers M, Debongnie J-F, Beckers P, Pure equilibrium tetrahedral finite elements for global error estimation by dual analysis. *Int. J. Num. Meth. Engng*. (2009) **81,** 513-536.